The Earth's exosphere and its response to space weather

Primary Author:
Hyunju Connor, NASA Goddard Space Flight Center

Co-Authors:
Dolon Bhattacharyya[1], Seth Claudepierre[2], Gonzalo Cucho-Padin[3], Jaewoong Jung[4], Dayeh Maher[5], Edwin Mierkiewicz[6], Susan Nossal[7], Kevin Pham[8], Eric Sutton[9], and Yongliang Zhang[10]

Affiliations:
[1]Laboratory for Atmospheric and Space Physics, [2]University of California - Los Angeles, [3]NASA Goddard Space Flight Center, [4]University of Alaska Fairbanks, [5]Southwest Research Institute, [6]Embry-Riddle University, [7]University of Wisconsin - Madison, [8]NCAR/HAO, [9]University of Colorado Boulder, and [10]JHU/APL

Synopsis:
Neutral-Plasma charge exchange is a fundamental physical process that occurs ubiquitously across the universe. In geospace, charge exchange occurs in the Earth's topside ionosphere, polar wind, plasmasphere, inner magnetosphere, and magnetosheath. Past and current space missions have profiled plasma and electromagnetic characteristics in various parts of the Earth's magnetospheric system. However, observations of the exosphere, i.e., neutrals above 500 km altitude, are still sparse and, in some regions, non-existent, which limits our understanding of the neutral contribution to the overall dynamics of the geospace environment.

Cold exospheric neutrals (< 10 eV) play an important role in the Sun-Earth interaction. Variability of exospheric density provides key information of the Earth's atmospheric loss under dynamic space environment conditions. Various neutral species and their density variations in the polar wind can alter ion outflow patterns, modifying global magnetospheric dynamics. Exospheric neutrals also provide an energy sink for the inner magnetosphere by creating Energetic Neutral Atoms (ENAs) through charge exchange with high-energy ring current ions, which subsequently leave our geospace system unimpeded by magnetic fields. Exospheric neutrals also provide a means to observe the global interaction of the solar wind – magnetosphere, through global imaging of the system via ENAs (e.g., the TWINS and IMAGE missions) and soft X-rays (e.g., the upcoming LEXI and SMILE missions), the byproducts of neutral-plasma charge exchange.

In the coming decade, we advocate that our community needs to increase our exploration of the neutral populations in the outermost reaches of the Earth's atmosphere. It is imperative that we improve both in-situ and remote-sensing technologies for measuring key neutral species in our exosphere. We also encourage dedicated exosphere missions and to stimulate model developments of our exosphere and its interaction with the co-located magnetospheric system and neighboring Ionosphere - Thermosphere - Mesosphere system.

1. Introduction

We lose part of our atmosphere everyday due to the Sun – Earth interaction. The Earth's exosphere connects our atmosphere to interplanetary space, and thus holds key information on this loss mechanism. The Earth's exospheric neutrals originate from the Earth's upper atmosphere and start ~500 km altitude, where neutral – neutral collisions effectively end. Above ~1500 km altitude, Hydrogen is the most dominant species, followed by Helium and Oxygen. Exospheric neutrals generally follow Newtonian motion under gravity, unlike the co-located plasma that is governed by electromagnetic forces. Depending on their velocities at the exobase (~500 km), some neutrals follow ballistic trajectories, some escape the system on hyperbolic trajectories, and some orbit the Earth above the exobase as satellite atoms, after being energized by charge exchange collisions with ionized species like H^+ and O^+ in the plasmasphere, polar wind, and ionosphere (Beth et al., 2014; Qin & Waldrop, 2016). Through their journey, some neutrals are lost to the interplanetary space by solar Extreme Ultraviolet (EUV) photoionization and by charge exchange with magnetospheric and interplanetary plasmas. During dynamic space environment conditions, physical processes like upper atmospheric heating, thermal evaporation, neutral-neutral collision, ion-neutral charge exchange, and photoionization occur in complex ways, causing temporal and spatial variations of exospheric density, and subsequently modifying atmospheric loss and neutral-plasma charge exchange across the entire geospace system. **Study of the exospheric density structure and its responses to various space conditions is key to understanding the past, current, and future of the Earth's atmosphere, advancing our knowledge of Sun – Earth interaction and the evolution of other planetary atmospheres**.

Exospheric neutrals also provide a means to remotely sense the global interaction of solar wind and the Earth's magnetospheric system through neural-plasma charge exchange. The TWINS and IMAGES missions have provided global images of the inner magnetosphere by measuring ENAs created from the charge exchange between inner magnetospheric plasma and exospheric neutrals (Figure 1a). The upcoming LEXI and SMILE missions will provide global images of the Earth's dayside systems by measuring X-ray photons emitted from the charge exchange between highly charged solar wind ions and exospheric neutrals (Figure 1b). Changes in these ENA and X-ray images can be interpreted as the plasma density variations caused by time-varying solar wind conditions, assuming a static terrestrial exosphere. However, recent studies (Cucho-Padin & Waldrop 2019; Qin et al., 2017; Zoennchen et al., 2017) revealed that our exosphere is quite dynamic. The assumption of a steady-state exosphere may not be applicable when interpreting the ENA and soft X-ray observations, especially during a geomagnetic storm. **Understanding the exospheric response to space weather is key to properly interpreting pre-existing and future remote-sensing datasets and thus to advancing our understanding of the solar wind – magnetosphere interaction.**

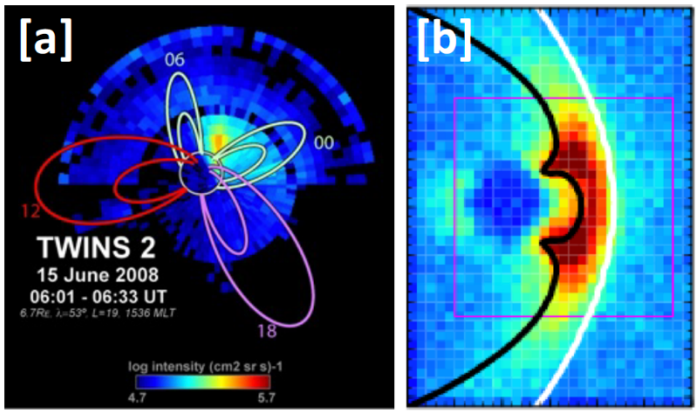

Figure 1 (a) TWINS ENA image of inner magnetosphere (TWINS website) (b) Simulated soft X-ray image of the Earth's dayside system

2. Science Questions for the Next Decade

The exospheric density distribution and its variability around the Earth are largely unknown due to the severe lack of simultaneous and global observations of the exosphere under various geomagnetic activities. In the next decade, we encourage our community to close this key knowledge gap by addressing the following questions.

2.1. How is the exospheric neutral density distributed around the Earth?

The direct, in-situ measurement of low-energy, low-density hydrogen has been notoriously difficult (Mitchell et al., 2016; Kepko et al., 2018). Previous investigations have been forced to rely on remote sensing observations of the geocorona (Baluikin et al., 2019; Kameda et al., 2017; Zoennchen et al., 2015), soft X-rays (Connor & Carter 2019; Jung et al., 2022), and ENAs (Fuselier et al., 2010; 2020). Figure 2 compares the dayside exospheric neutral density along the Sun-Earth line, obtained from the previous studies, where a large density discrepancy is noted. For example, the neutral density at 10 Earth radii (R_E) ranges from 4 to 59 cm^{-3}, i..e., over 1300% relative difference. Such large discrepancies can be explained as follows. First, the various sources observed different exospheric regions from different vantage points under different space environments. Exospheric conditions in each observational period may be different. Second, the line-of-sight observations provide a proxy of column exosphere density but hold no information about the density distribution along the look direction. Various analytic functions were assumed for the density distribution, fitted to the datasets for calculating coefficients of the functions, and then utilized with the coefficients for neutral density estimation. Last, geocorona, soft X-ray, and ENA observations are the results of different physical processes – resonant scattering of solar photons (geocorona) and neutral charge exchange with plasmas of different origins (soft X-ray and ENA). Various inversion and background removal techniques are needed for the density estimation, which makes cross calibration exceptionally challenging. With limited observations and technologies, we do not fully understand the general conditions of our exosphere. Subsequently, our understanding of the physical processes that govern the exosphere and neutral-plasma interaction remain poorly characterized. For the next decade, it is imperative that we uncover the fundamental states of our exosphere under various geospace environmental conditions.

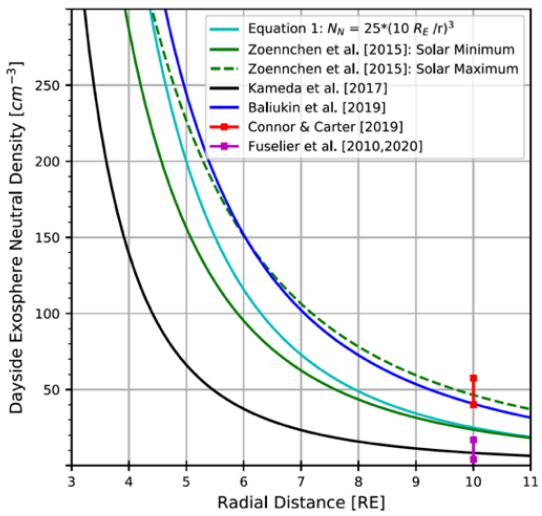

Figure 2 Comparison of the dayside exospheric neutral densities along the Sun – Earth line, obtained from various sources (Connor et al. 2021)

2.2. How and why does the density vary due to solar irradiance?

Solar irradiance plays a significant role in determining the exospheric density. On one hand, strong EUV radiation during solar maximum heats the thermosphere and strengthens the upwelling and

escape of neutrals above the exobase, which eventually replenishes the Earth's exosphere. On the other hand, strong solar EUV irradiance during solar maximum efficiently ionizes exospheric neutrals and decreases its density. Moreover, the increased solar radiation pressure during solar maximum redistributes the exospheric particles in a non-symmetric way, strongly enhancing the densities in the noon and midnight sectors (Beth et al., 2016). Previous studies presented a variety of exospheric responses over the course of a solar cycle. Zoennchen et al. (2015) showed increasing exospheric density with increasing solar irradiance (Figure 3), while Waldrop and Paxton (2013) and Baliukin et al. (2019) showed a decrease of exospheric density. Fuselier et al. (2010; 2020) also reported a minimal impact of solar irradiance on the exosphere. Despite a unanimous agreement of solar irradiance control over the exosphere, where, how much, and how long the exospheric density changes under solar irradiance variation are still poorly understood. We advocate that the community obtains a better understanding of exospheric responses to the continuously varying solar irradiance and the physics that governs the exospheric behavior.

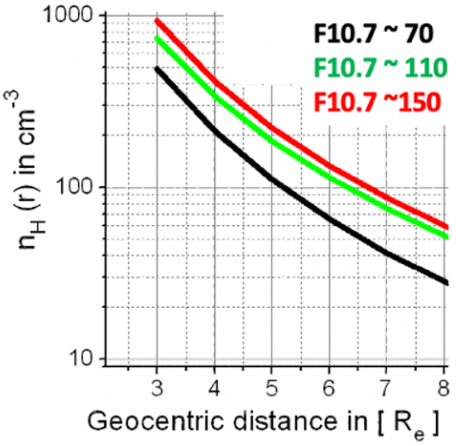

Figure 3. Averaged Hydrogen density profile obtained from the TWINS geocorona observations (Zoennchen et al. 2015)

2.3. How and why does the density distribution vary during a geomagnetic storm?

Research on storm-driven exospheric variability has rapidly progressed in recent years, by utilizing the TWINS geocorona observations. Bailey & Gruntman (2013) reported the increase of exospheric hydrogen density (N_H) by 6~17% in a region of 3-8 R_E radial distance by extracting the density from the TWINS geocorona observations of 5 geomagnetic storms. Zoennchen et al. (2017) also reported the similar density increase of 9 – 23 % in the same radial distances by considering the variation of the geocoronal column brightness ($\Delta I_{Ly\text{-}\alpha}$) as a proxy of column hydrogen density variation (ΔN_H). Their analysis of 8 geomagnetic storms showed that the enhancement of geocoronal emission tends to decrease with increasing storm intensity parameterized by minimum Dst (see blue points in Figure 4), implying a complex response of our exosphere to a geomagnetic storm. Cucho-Padin & Waldrop (2019) presented additional intriguing storm-time behaviors by applying a tomographic method to the TWINS storm-time geocorona observations. They reported that N_H enhances by ~15% at 3R_E geocentric distance soon after the minimum Dst, and the density enhancement propagates outward. The N_H enhancement and propagation during a geomagnetic storm will change the neutral-plasma charge exchange in a complex way, affecting the ring current

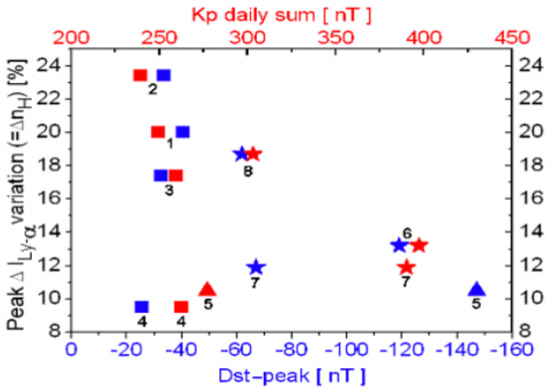

Figure 4. Peak enhancement of Ly-α column brightness vs minimum Dst (blue) for 8 geomagnetic storms

dynamics and the neutral escapes to interplanetary space. It is thus crucial that our community addresses the question of storm-time exospheric variability, its impact on the co-located magnetospheric plasma populations, and the physics behind such behaviors.

2.4. How does the exosphere respond to a changing climate?

Whole atmosphere studies indicate that climate change processes impact even the uppermost regions of the atmosphere and that there are vertical footprints of climate change processes in the upper atmosphere. Carbon dioxide increases lead to rapid cooling in the thermosphere accompanying the warming of the troposphere, as well as to changes in upper atmospheric densities and constituent concentrations (Roble and Dickinson, 1989; Solomon et al., 2018, 2019). The simulated temperature decrease in the upper thermosphere (-2.8 K per decade at low solar activity) is of larger magnitude than the simulated warming at the surface (+0.2 K per decade) during the time interval of the early 2000s compared with the early 1970s.

Additionally, upper thermospheric hydrogen simulations predict increases due both to carbon dioxide cooling and to increases in the source species for hydrogen (Nossal et al., 2016). Hydrogen is a by-product of species such as water vapor that has been observed to increase in the stratosphere and mesosphere through satellite observations by SABER and the MLS (Yue et al., 2019). Investigation of the response of exospheric temperature and hydrogen can offer potential vertical footprints to better understand climate change processes and coupling between the exosphere to lower altitudes. Additionally, changes to hydrogen due to increases in greenhouse gases can impact the plasmasphere-neutral atmosphere coupling and associated processes (Krall et al., 2018).

3. Recommendations for the Next Decade

3.1. Developing technologies and techniques for detecting exospheric neutrals

Our community must improve both in-situ and remote-sensing technologies for measuring neutral species in our exosphere (e.g., Hydrogen, Helium, and Oxygen).

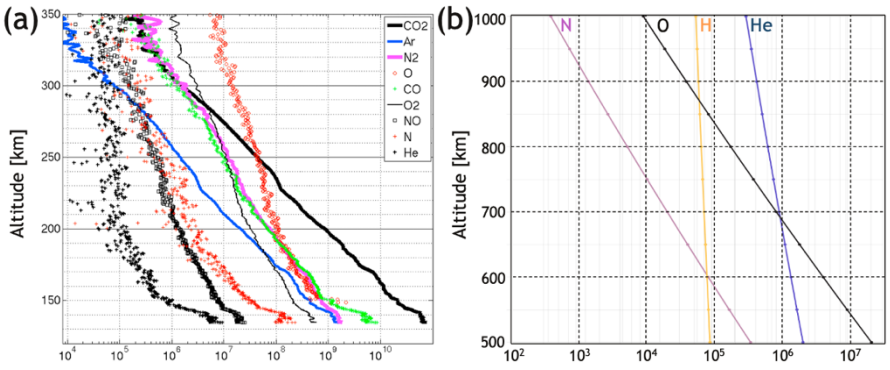

Figure 5 (a) Measurements of Martian atmosphere by the MAVEN Neutral Mass Spectrometer (Mahaffy et al. 2015), (b) The Earth's exospheric density from the MSIS empirical model.

First, the neutral mass spectrometer technology needs to be improved for directly measuring tenuous exospheric neutrals. Figure 5a shows the measurement range of the high-heritage neutral mass spectrometer that was flown on the Mars Atmosphere and Volatile Evolution (MAVEN) and is selected for the Geospace Dynamics Constellation (GDC). Figure 5b shows density ranges of

key neutral species in the altitude of 500 – 1000 km, obtained from the MSIS empirical model. The current technology limits in-situ observation of the outer exosphere where the neutral density goes below 10^4 cm^{-3} due to poor signal-to-noise ratios. Additionally, hydrogen atoms, the most abundant exospheric species, are very difficult to detect with current technologies because hydrogens are converted to water within the instrument due to its high reactivity with oxygens. Additionally, satellite outgassing also interferes with the observed hydrogen signal since it produces hydrogen fragments when ionizing hydrogen atoms for detection. In-situ measurement techniques must be improved.

Second, various remote-sensing techniques should be implemented for estimating hydrogen density with high accuracy. New spatial heterodyne spectroscopy (SHS) techniques enable space-based high spectral resolution measurements of geocoronal Lyman series emission lines. These multi-line observations can provide detailed information about hydrogen's upward evaporative flux, vertical column density and kinetic partition function populations. The application of highly sensitive Fabry-Perot (and SHS) techniques has also opened new ground-based remote sensing avenues, including observations of sub Rayleigh Balmer β emission (Mierkiewicz, 2021; Roesler et al., 2014; Gardner et al., 2017). By utilizing the Bamer-lines ground data and the Lyman-lines space data, we can constrain forward-model retrieved hydrogen density profiles (e.g., Bishop et al., 2004; Gardner et al., 2017). A fully implemented multi-line retrieval approach over the next decade will improve H(z) retrievals from stand-alone single line data.

Third, a Far UltraViolet (FUV) instrument should be utilized to measure exospheric hydrogen and oxygen. The TIMED/GUVI (Paxton et al., 1999; Christensen et al., 2003) Ly-α FUV limb data have been successfully used in estimating the hydrogen density profiles during a geomagnetic storm (Qin et al., 2017). Zhang et al. (2022) found that the GUVI O 130.4 nm limb radiance is well correlated with thermospheric neutral density where O is the dominant species. The limb 130.4 nm radiance can be used to monitor the change of atomic O density in the thermosphere (Figure 6). Both Ly-α and O 130.4nm are significantly contributed by resonant scattering of bright solar emissions (Meier et al., 1982, 1991). This suggests that the FUV instrument like TIMED/GUVI is feasible to detect both Ly-α and O 130.4 nm limb emissions at exosphere altitudes. These limb emissions enable the extraction of both O and H density profiles. This will not only fill our knowledge gaps but also open a way to understand the exosphere dynamics and its impact on ring current ion loss due to charge exchange.

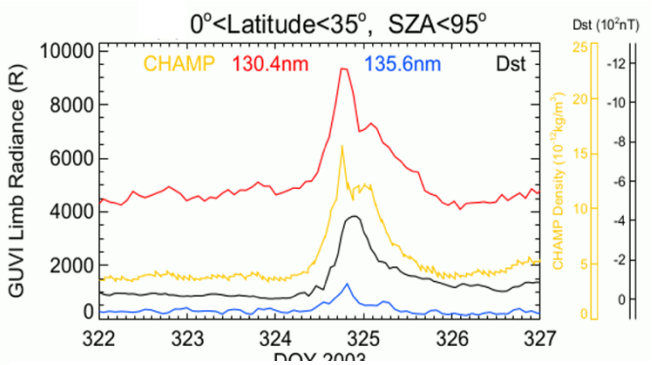

Figure 6. Dayside orbital average of TIMED/GUVI dayside limb (~400 km tangent altitude and between latitudes 0° and 35°). 130.4 nm radiance (red line), 135.6 nm radiance (blue line), dayside orbital average of CHAMP neutral density (yellow line, between 0° and 35°) at 400km, and Dst index (black line) during a geomagnetic storm on 18-23 Nov 2003. (Zhang et al. 2022)

Last, the density extraction techniques should be improved for remote-sensing data analysis. A means of inferring the global and time-dependent H density distribution across the vast exospheric region is through observations of the resonantly scattered solar Ly-α emission by exospheric H atoms. Because Ly-α photon scattering involves the ground state of atomic H,

incident photons can undergo multiple re-scatterings by ambient H atoms before being detected by a space-based sensor. Analysis of such "optically thick" emission data in terms of the unknown H density distribution requires the inversion of sophisticated forward models of photon transport, or radiative transfer (RT), that feature several intrinsic assumptions like spherical geometry, asymmetric illumination, and isothermal and Maxwellian properties for the emitters (Beth et al., 2016; Bhattacharyya et al., 2017; Meier, 1991). This, however, is not entirely representative of the actual characteristics of terrestrial exospheres as they might be asymmetric in nature (Hodges, 1994; Zoennchen et al., 2015; Bhattacharyya et al., 2017), may not be isothermal, especially at lower altitudes (Bhattacharyya et al., 2020), and is likely to contain non-thermal atoms (Qin and Waldrop, 2016; Bhattacharyya et al., 2015; Chaufray et al., 2012). Thus, future efforts in remote sensing should focus on developing 2-D/3-D RT models that enable the estimation of non-isothermal and asymmetric H density distributions in the terrestrial exosphere which has been previously observed in a handful of wide-field images of Earth's extended exosphere (Baliukin et al., 2019; Carruthers et al., 1976, Kameda et al., 2017).

When the number density of exospheric H atoms is sufficiently low, the Ly-α scattering medium can be considered "optically thin." In that case, the column-integrated Ly-α emission observed by a space-based detector is linearly related to the volumetric H density. Such a condition enables the formulation of an inverse problem that has been solved using tomographic techniques (Cucho-Padin and Waldrop, 2018) and parametric estimation (Zoennchen et al., 2015) at Earth. Notwithstanding, the optically thin region is not only illuminated by solar photons but also by scattered photons from lower altitudes, where the exosphere is optically thick. This phenomenon, known as albedo, must be accounted for reliable estimation of exospheric density distributions in the optically thin regions. To do so, an RT model, with aforementioned requirements of dimensionality, is needed to correct the estimation.

3.2. Planning various exospheric missions

Global Ly-α Imager for the Dynamic Exosphere (GLIDE) is the upcoming NASA mission for studying variability of the terrestrial exosphere. The Ly-α instrument on GLIDE will provide global geocoronal images after its launch to the L1 Lagrange point in 2025. However, due to its vantage point, GLIDE will miss day-night geocorona variations that holds key information of the upper atmospheric heating near cusps and auroral ovals, and its subsequent impact on the exosphere. Additionally, GLIDE will estimate exospheric density below ~6000 km altitude from the limb brightening of geocorona by utilizing notoriously challenging inverse conversion techniques under various assumptions (e.g., solar Ly-α sources, interplanetary Ly-α background, photon scattering rates and directions). Their observations can create a large density error without additional observations that provide constraints on the density estimation. A single spacecraft won't fully address the science questions in section 3.

We advocate multi-point exospheric observations from space and ground. We also advocate combination of the in-situ and remote-sensing observations for revealing local and global states of exospheres and thus enabling multi-scale study of exospheric dynamics. Such observational strategies have been widely implemented and successful for understanding the electromagnetic dynamics of near-Earth plasmas (e.g., the multi-satellite observations like Clusters, THEMIS, and TWINS, and their conjunction studies with ground observatories like SuperDARN, SuperMAG, and all sky imagers). Similar observation strategies should be applied to the exosphere. The GLIDE and GDC missions scheduled in the coming decade provide excellent opportunities to achieve these strategies.

We suggest concurrent geocorona observations from various vantage points while GLIDE is operational. At least one additional space mission is recommended to observe day-night geocoronal variation. Observations from two different vantage points will enable us to extract three-dimensional exospheric density using tomographic approaches (e.g., Cucho-Padin & Waldrop 2019) that uses less assumptions on the neutral density estimations. Ground-based Balmer-line observations (e.g., Mierkierwicz, 2021) can also provide additional constraints for the density extraction techniques and thus improve the exospheric density profiles.

We also advocate in-situ observations of helium density in the 700 – 1500 km altitude while GDC is operational. Helium is a major neutral species in the altitude of 700 ~ 1500 km and its density varies within the detection capability of current technologies (Figure 5). The helium density measurements at these altitudes will reveal variability and physics of the inner exosphere, the optically thick region where density extraction from the remote-sensing dataset becomes exceptionally challenging. Additionally, helium is a noble gas. Its inertness makes helium an ideal tracer to understand the physics of the coupled upper atmosphere - exosphere system. The neutral mass spectrometers on GDC satellites will provide local and global measurements of helium density at ~350 km altitudes after their expected launch in late 2027. In combination with the GDC thermospheric helium dataset, the exospheric helium measurements will provide a unique opportunity to study the collisional-to-collisionless transition region and subsequently improve the coupled upper atmosphere – exosphere modeling.

3.3. Developing exosphere models

Physics-based exosphere modeling is a great way to understand the global density distribution, its variability, and its physical origin and drivers. The Monte-Carlo approach (Hodges 1994; Baliukin et al., 2019; references therein) is widely used to simulate the collisionless regime of our atmosphere. These models first calculate trajectories of neutral atoms by considering various force terms like gravitational acceleration, solar radiative pressure, and Coriolis and centrifugal accelerations. Then, they calculate phase-space densities of traced particles by considering conditions of the upper atmosphere and exobase as well as various source/loss mechanisms along the particle trajectories (e.g., photoionization, neutral-neutral collision, neutral-plasma charge exchange). However, previous models focused only on the static exosphere under steady space weather conditions; for example, a fixed F10.7 solar irradiance index at equinox and solstice (Hodges, 1994) and a homogeneous exobase condition with no spatial and temporal variation (Baliukin et al., 2019).

No modeling studies address exospheric variabilities under continuously varying solar irradiation and during a geomagnetic storm. This is partly because scientists lacked the knowledge of exospheric variability due to the limited observations, and partly because the time-varying exobase input to drive Monte-Carlo simulations was difficult to obtain before the 1990s when the exosphere modeling studies (Hodges, 1994; references therein) were blossoming. Recent TWINS geocoronal observations have started to reveal the exospheric variabilities. Physics-based upper atmosphere models like WACCAM-X, GITM, and TIME-GCM have been greatly improved in the past decade, providing dynamic exobase conditions in response to solar irradiations and geomagnetic storms and the potential to simulate the response to climate change. Modeling investigations of exospheric variability, accounting for the dynamic atmosphere – exosphere coupling, are a natural next step for the coming decade.

References

Baliukin, I., Bertaux, J. -L., Quémerais, E., Izmodenov, V., & Schmidt, W. (2019). SWAN/SOHO Lyman-α mapping: The hydrogen geocorona extends well beyond the Moon. Journal of Geophysical Research: Space Physics, 124, 861–885. https://doi.org/10.1029/2018JA026136

Bailey, J., and M. Gruntman (2013), Observations of exosphere variations during geomagnetic storms, Geophys. Res. Lett, 40, 1907–1911, doi:10.1002/grl.50443.

Bhattacharyya, D., J. T. Clarke, J.-L. Bertaux, J.-Y. Chaufray, and M. Mayyasi (2015), A strong seasonal dependence in the Martian hydrogen exosphere, Geophys. Res. Lett., 42, 8678–8685, doi:10.1002/2015GL065804.

Bhattacharyya, D., Clarke, J. T., Chaufray, J. Y., Mayyasi, M., Bertaux, J. L., Chaffin, M. S., … Villanueva, G. L. (2017). Seasonal changes in hydrogen escape from mars through analysis of HST observations of the Martian exosphere near perihelion. *Journal of Geophysical Research: Space Physics*, 122, 11,756–11,764. https://doi.org/10.1002/ 2017JA024572

D. Bhattacharyya, J.Y. Chaufray, M. Mayyasi, J.T. Clarke, S. Stone, R.V. Yelle, W. Pryor, J.L. Bertaux, J. Deighan, S.K. Jain, N.M. Schneider, (2020). Two-dimensional model for the martian exosphere: Applications to hydrogen and deuterium Lyman α observations, *Icarus*

Beth, A., P. Garnier, D. Toublanc, I. Dandouras, C. Mazelle, and A. Kotova, Modeling the satellite particle population in the planetary exospheres: application to Earth, Titan and Mars. ICARUS 227, 21–36 (2014).

Beth, A., P Garnier, D Toublanc, I Dandouras, C Mazelle (2016), Theory for planetary exospheres: III. Radiation pressure effect on the Circular Restricted Three Body Problem and its implication on planetary atmospheres, *Icarus* 280, 415-423

Bishop, J., Mierkiewicz, E. J., Roesler, F. L., Gomez, J. F., & Morales, C. (2004), Data-model comparison search analysis of coincident PBO Balmer α, EURD Lyman β geocoronal measurements from March 2000. *Journal of Geophysical Research*, *109*, A05307. https://doi.org/10.1029/2003JA010165

Carruthers, G. R., Page, T., & Meier, R. R. (1976). Apollo 16 Lyman alpha imagery of the hydrogen geocorona. *Journal of Geophysical Research*, 81(10), 1664–1672.

Chaufray, J.-Y., Bertaux, J.-L., and Leblanc, F. (2012), First observation of the Venus UV dayglow at limb from SPICAV/VEX, *Geophys. Res. Lett.*, 39, L20201, https:/doi.org/10.1029/2012GL053626

Connor, H. K. and Carter, J. A. (2019), Exospheric neutral hydrogen density at the 10 RE subsolar point deduced from XMM-Newton X-ray observations, Journal of Geophysical Research: Space Physics, doi:10.1029/2018JA026187

Connor, H. K. and Sibeck, D. G. and Collier, M. R. and Baliukin, I. I. and Branduardi-Raymont, G. and Brandt, P. C. and Buzulukova, N. Y. and Collado-Vega, Y. M. and Escoubet, C. P. and Fok, M.-C. and Hsieh, S.-Y. and Jung, J. and Kameda, S. and Kuntz, K. "Soft X-ray and ENA Imaging of the Earth's Dayside Magnetosphere" Journal of Geophysical Research: Space Physics , v.126 , 2021. https://doi.org/10.1029/2020JA028816

Cucho-Padin, G., & Waldrop, L. (2018). Tomographic estimation of exospheric hydrogen density distributions. *Journal of Geophysical Research: Space Physics*, 123, 5119– 5139. https://doi.org/10.1029/2018JA025323

Cucho-Padin, G., & Waldrop, L. (2019). Time-dependent response of the terrestrial exosphere to a geomagnetic storm. Geophysical Research Letters, 46, 11661– 11670.

Christensen, A. B., et al. (2003), Initial observations with the Global Ultraviolet Imager (GUVI) in the NASA TIMED satellite mission, *J. Geophys. Res.*, 108, 1451, https://doi.org/10.1029/2003JA009918

Fuselier, S. A., Funsten, H. O., Heirtzler, D., Janzen, P., Kucharek, H., McComas, D. J., et al. (2010). Energetic neutral atoms from the Earth's sub-solar magnetopause. Geophysical Research Letters, 37, L13101. https://doi.org/10.1029/2010GL044140

Fuselier, S. A., Dayeh, M. A., Galli, A., Funsten, H. O., Schwadron, N. A., Petrinec, S. M., et al. (2020). Neutral atom imaging of the solar wind – magnetosphere - exosphere interaction near the subsolar magnetopause. Geophysical Research Letters, 47, e2020GL089362. https://doi.org/10.1029/2020GL089362

Gardner, D. D., Mierkiewicz, E. J., Roesler, F. L., Nossal, S. M., & Haffner, L. M. (2017), Constraining Balmer alpha fine structure excitation measured in geocoronal hydrogen observations. Journal of Geophysical Research: Space Physics, 122, 10,727–10,747. https://doi.org/10.1002/2017JA024055

Hodges, R. R., Jr. (1994). Monte Carlo simulation of the terrestrial hydrogen exosphere. Journal of Geophysical Research, 99, 23229–23247.

Ilie, R., Skoug, R., Funsten, H. O., Liemohn, M. W., Bailey, J. J., & Gruntman, M. (2013). The impact of geocoronal density on ring current development. Journal of Atmospheric and Solar-Terrestrial Physics, 99, 92, 103

Jung, J., Connor, H. K., Carter, J. A., Koutroumpa, D., Pagani, C., & Kuntz, K. D. (2022). Solar minimum exospheric neutral density near the subsolar magnetopause estimated from the XMM soft X-ray observations on 12 November 2008. Journal of Geophysical Research: Space Physics, 127, e2021JA029676. https://doi.org/10.1029/2021JA029676.

Kameda, S., Ikezawa, S., Sato, M., Kuwabara, M., Osada, N., Murakami, G., Fujimoto, M. (2017). Ecliptic north-south symmetry of hydrogen geocorona. Geophysical Research Letters, 44, 11,706– 11,712. https://doi.org/10.1002/2017GL075915

Kepko, Larry, Luis Santos, Chuck Clagett, Behnam Azimi, Dean Chai, Alan Cudmore, Scott Starin, James Marshall, John Lucas, Dellingr: Reliability lessons learned from on-orbit, small satellite conference, 2018.

Krall, J., Glocer, A., Fok, M.-C., Nossal, S. M., & Huba, J. D. (2018). The unknown hydrogen exosphere: Space weather implications. *Space Weather*, 16, 205– 215. https://doi.org/10.1002/2017SW001780

Mahaffy, P. R., M. Benna, M. Elrod, R. V. Yelle, S. W. Bougher, S. W. Stone, and B. M. Jakosky (2015), Structure and composition of the neutral upper atmosphere of Mars from the MAVEN NGIMS investigation, Geophys. Res. Lett., 42, 8951–8957, doi:10.1002/2015GL065329

Meier, R.R. Ultraviolet spectroscopy and remote sensing of the upper atmosphere. *Space Sci Rev* 58, 1–185 (1991). https://doi.org/10.1007/BF01206000

Meier, R. R., Conway, R. R., Feldman, P. D., Strickland, D. J., and Gentieu, E. P. (1982), Analysis of nitrogen and oxygen far ultraviolet auroral emissions, *J. Geophys. Res.*, 87(A4), 2444– 2452, https://doi.org/10.1029/JA087iA04p02444.

Mierkiewicz, E.J. (2021), "Neutral Hydrogen in the Terrestrial Thermosphere and Exosphere: A Ground-Based Perspective," in Upper Atmosphere Dynamics and Energetics, Book Editor(s): W. Wang, Y. Zhang, and L.J. Paxton, John Wiley & Sons, Inc., doi:10.1002/9781119815631.ch8

Mitchell, D. G., Brandt, P. C., Westlake, J. H., Jaskulek, S. E., Andrews, G. B., and Nelson, K. S. (2016), Energetic particle imaging: The evolution of techniques in imaging high-energy neutral atom emissions, J. Geophys. Res. Space Physics, 121, 8804– 8820, doi:10.1002/2016JA022586.

Nossal, S. M., Qian, L., Solomon, S. C., Burns, A. G., and Wang, W. (2016), Thermospheric hydrogen response to increases in greenhouse gases, *J. Geophys. Res. Space Physics*, 121, 3545–3554, https://doi.org/10.1002/2015JA02208

Paxton, L. J., et al. (1999), Global ultraviolet imager (GUVI): Measuring composition and energy inputs for the NASA Thermosphere Ionosphere Mesosphere Energetics and Dynamics (TIMED) mission, *Optical Spectroscopic Techniques and Instrumentation for Atmospheric and Space Research III–Proceedings of SPIE*, page 256–276, 19 – 21 July 1999, Denver, Colorado

Qin, J., and L. Waldrop, Non-thermal hydrogen atoms in the terrestrial upper thermosphere, Nature Communications, 7, 13,655, doi:10.1038/ncomms13655, 2016.

Qin, J., L. Waldrop, and J. J. Makela, Redistribution of H atoms in the upper atmosphere during geomagnetic storms, Journal of Geophysical Research: Space Physics, 122(10), 10,610–686,693, doi:10.1002/2017JA024489, 2017.

Roble, R. G. and Dickinson, R. E. (1989) How will changes in carbon dioxide and methane modify the mean structure of the mesosphere and thermosphere? *Geophys. Res. Le*tt. 16. https://doi.org/10.1029/GL016i012p01441

Roesler, F. L., E. J. Mierkiewicz, and S. M. Nossal (2014), The geocoronal H α cascade component determined from geocoronal H β intensity measurements, J. Geophys. Res. Space Physics, 119, 6642–6647, doi:10.1002/2014JA020026

Solomon, S. C., Liu, H.-L., Marsh, D. R., McInerney, J. M., Qian, L., & Vitt, F. M. (2018). Whole atmosphere simulation of anthropogenic climate change. *Geophysical Research Letters*, 45, 1567– 1576. https://doi.org/10.1002/2017GL076950

Solomon, S. C., Liu, H.-L., Marsh, D. R., McInerney, J. M., Qian, L., & Vitt, F. M. (2019). Whole atmosphere climate change: Dependence on solar activity. *Journal of Geophysical Research: Space Physics*, 124, 3799– 3809. https://doi.org/10.1029/2019JA026678

Sutton, E. K., J. P. Thayer, W. Wang, S. C. Solomon, X. Liu, and B. T. Foster (2015), A self-consistent model of helium in the thermosphere, J. Geophys. Res. Space Physics, 120, 6884–6900, doi:10.1002/2015JA021223.

Waldrop, L., and L. J. Paxton (2013), Lyman-alpha airglow emission: Implications for atomic hydrogen geocorona variability with solar cycle, J. Geophys. Res. Space Physics, 118, 5874–5890, doi:10.1002/jgra.50496.

Yue., J., Russell, J., Gan, Q., Wang, T., Rong, P., Garcia, R., & Mlynczak, M. (2019). Increasing Water Vapor in the Stratosphere and Mesosphere After 2002. *Geophysical Research Letters*, 46, 13452– 13460. https://doi.org/10.1029/2019GL084973

Y. Zhang, L. J. Paxton, R. Schaefer (2022), Thermospheric density enhancement and limb O 130.4 nm radiance increase during geomagnetic storms, Journal of Atmospheric and Solar-Terrestrial Physics, Volume 229

Zoennchen, J. H., Nass, U., and Fahr, H. J. (2015), Terrestrial exospheric hydrogen density distributions under solar minimum and solar maximum conditions observed by the TWINS stereo mission, Ann. Geophys., 33, 413–426, doi:10.5194/angeo-33-413-2015, 2015.

Zoennchen, J. H., Nass, U., Fahr, H. J., & Goldstein, J. (2017). The response of the H geocorona between 3 and 8 Re to geomagnetic disturbances studied using TWINS stereo Lyman-alpha data. Annales Geophysicae, 35(1), 171–179. https://doi.org/10.5194/angeo-35-171-2017.